Advances in Science and Technology Research Journal

Advances in Science and Technology Research Journal, 2026, 20(4), 373–388
https://doi.org/10.12913/22998624/215395
ISSN 2299-8624, License CC-BY 4.0

Received: 2025.10.23
Accepted: 2026.02.15
Published: 2026.03.01

Solar photocatalytic treatment of wastewater contaminated with pesticides: Application of artificial neural network modelling

Yasmen Mustafa[1*], Ahmad Hassan[2], Saif Alsabti[1]

[1] Department of Medical Instrumentation Engineering Techniques, College of Technical Engineering, Al-Bayan University, Baghdad, Iraq
[2] Department of Civil Engineering, College of Engineering, Al Iraqia University, Baghdad, Iraq
* Corresponding author's e-mail: yasmen.mustafa@gmail.com

ASTRACT

Homogeneous and heterogeneous photocatalysis systems were used to treat water contaminated with three pesticides, atrazine (ATZ), diazinon (DIZ), and alachlor (ALC). A pilot-scale plant powered by solar energy, consisting of compound parabolic collectors (CPCs), was used. The effect of H_2O_2 concentration from 200 to 2400 mg/L, Fe^{+2} from 5 to 30 mg/L, and TiO_2 from 100 to 500 mg/L was studied to find their effects on the degradation efficiency. The concentrations of the parent pollutants rapidly declined to zero for ALC and DIZ in the initial stages of the experiment and were converted into intermediate products. The chemical oxygen demand (COD) removal efficiency for the homogeneous photocatalytic process at the optimal dosage was 45%, 74%, and 80% for ATZ, ALC, and DIZ, respectively. In comparison, the heterogeneous photocatalytic system showed removal efficiencies of 43%, 73%, and 76% for the same compounds. The single, binary, and ternary pesticide mixtures were tested in a homogeneous system. The results show that ATZ reduces oxidation of the mixture when combined with other pesticides. An artificial neural network was employed to predict the experimental results. The model demonstrated a good fit with the experimental results.

Keywords: advanced oxidation processes, photo-Fenton, TiO_2, atrazine, diazinon, alachlor.

INTRODUCTION

Solar energy is one of the most promising renewable resources, offering a clean, abundant, and sustainable alternative to conventional energy sources. Iraq, in particular, benefits from exceptionally high levels of solar radiation year-round, making it an ideal location to harness solar power for environmental applications. Among these, solar-driven advanced oxidation processes offer an effective and sustainable approach to addressing critical water pollution challenges. Water pollution represents a critical environmental challenge that causes severe effects on both human health and ecosystems. The release of toxic substances from industrial discharge, agricultural runoff, and other sources without proper treatment may degrade water quality. Pesticides have been employed in agriculture to protect crops from pests and diseases and to enhance both the yield and quality of fruits and vegetables. Globally, around 2 million tonnes of pesticides are used each year, of which 47.5% are herbicides, and 29.5% are insecticides [1–3]. The widespread use of pesticides can have severe consequences due to their persistent nature and potential for bio-magnification. Pesticides can contaminate air, water, soil, and entire ecosystems, leading to significant health risks for all living organisms.

Generally, herbicides are more commonly found in surface water than insecticides, reflecting their higher usage. The most frequently detected herbicides include atrazine, cyanazine, simazine, metolachlor, alachlor, and 2,4-D, among the most widely used in agriculture. As for insecticides, carbofuran and diazinon are the most commonly detected in surface water [4–6]. Atrazine (ATZ) is an herbicide of the chlorotriazine class, utilized

for controlling annual broadleaf and grassy weeds. Atrazine metabolites (deethyl atrazine, deisopropyl-atrazine, and diamino chlorotriazine) were found in the surface and groundwater as reported by Cleary et al. and Hu et al. [7, 8]. The hydroxyatrazine metabolite is commonly found in groundwater. The guideline value for atrazine and its metabolites is 0.1 mg/L, while the guideline value for hydroxyatrazine is 0.2 mg/L [9, 10].

Alachlor (ALC) is a pre- and post-emergence herbicide used to control annual broadleaf and grass weeds in maize and other crops. Numerous alachlor degradation products have been detected in soil. The guideline value is 0.02 mg/L [10]. Diazinon (DIZ) is an organophosphate insecticide that has been utilized since 1956 to control insects on field crops, vegetables, and fruits. As a result, farmers and workers may be exposed to DIZ through air, water, and food. Currently, there are no enforceable drinking water standards for diazinon. The U.S. EPA has issued a lifetime health advisory for diazinon in drinking water at 0.001 mg/L, but this guideline is not legally enforceable [11, 10]. In recent years, advanced oxidation processes (AOPs) have encountered significant attention for their effectiveness in degrading recalcitrant organic compounds. In AOP, hydroxyl radical ($OH^{\bullet}$) was generated, which is a highly reactive and nonselective substance that can break up the recalcitrant molecules and convert them into degradable substances such as CO_2 and H_2O. The hydroxyl radical is capable of reacting with nearly all classes of organic compounds, leading to partial mineralization and the formation of less harmful products [12].

Mixtures of ferrous iron and hydrogen peroxide are known as the Fenton reagent. The Fenton reaction is widely used for degrading organic pollutants. It involves the catalytic breakdown of hydrogen peroxide by reacting with iron salts, as shown in Equation 1. This process produces hydroxyl radicals, which are mainly responsible for breaking down contaminants [13].

$$Fe^{+2} + H_2O_2 \rightarrow Fe^{+3} + OH^- + OH^{\bullet} \quad (1)$$

One significant drawback of the Fenton process is that it aims for the total mineralization of organic pollutants. The intermediate product that evolved from the reaction, which produced mainly carboxylic and dicarboxylic acids, can form a stable iron complex with Fe^{+3}, shown in Equation 2, which inhibits the reaction with peroxide. As a result, the catalytic iron cycle stops before total mineralization is achieved.

$$Fe^{+3} + CH_3COO^- \rightarrow Fe[(CH_3COO)]^{+2} \quad (2)$$

In the presence of UV light (wavelengths <580 nm), ferric iron complexes absorb sufficient energy, leading to ligand-to-metal charge transfer (LMCT). In this process, an electron is transferred from the carboxylate ligand to the ferric ion, reducing Fe^{3+} back to $Fe^{2+}$and oxidizing the acetate ligand into an organic radical, as shown in Equation (3). The regeneration of Fe^{+2} promotes the decomposition of H_2O_2 to produce more $OH^{\bullet}$.

$$Fe[(CH_3COO)]^{+2} + hv \rightarrow Fe^{+2} + CH_2COO^{-\bullet} \quad (3)$$

The UV/Fe^{2+}/H_2O_2 process provides numerous benefits for degrading organic pollutants, such as its broad applicability, rapid mineralization rates, utilization of eco-friendly reagents, and production of fewer harmful by-products [14–16]. One of the leading advanced oxidation techniques involves the photo-excitation of semiconductor surfaces using ultraviolet-visible light. Titanium dioxide (TiO_2) is widely used in photocatalytic degradation due to its high activity, non-toxicity, affordability, chemical and biological stability, water insolubility, corrosion resistance, and accessibility compared to other materials [17].

When a semiconductor absorbs a photon with sufficient energy (equal to or greater than the band gap energy), an electron in the valence band gains energy and is excited to the conduction band, this process is called photonic excitation. The electron's movement to the conduction band leaves behind an empty state in the valence band, referred to as a hole (h^+).The electron-hole pair ($e^- + h^+$) refers to the creation of an electron in the conduction band and a corresponding hole in the valence band, which are generated together as a result of the absorption of a photon, Equation 4.

$$TiO_2 + hv \rightarrow TiO_2(e^- + h^+) \quad (4)$$

Holes in the valence band carry a positive charge and can interact with water molecules to produce hydroxyl radicals $OH^{\bullet}$ and hydrogen ions (H^+), Equation 5. Superoxide ions ($O_2^{-\bullet}$), was formed when the oxygen dissolved in water reacts with the electrons in the conduction band, Equation 6, which further reacts with water molecules to generate hydroxide ions (OH^-) and hydroperoxyl radicals ($HOO^{\bullet}$) Equation 7. These hydroperoxyl radicals then combine with H^+ ions to produce both hydroxyl radicals ($OH^{\bullet}$) and

hydroxide ions (OH^-) Equation 8. The holes in the valence band can also oxidize (OH^-) to form additional ($OH^\bullet$) radicals, Equation 9. Together, these processes lead to the generation of hydroxyl radicals ($OH^\bullet$), which attack pollutants present in the aqueous solution [18].

$$h^+ + H_2O \rightarrow OH^\bullet + H^+ \quad (5)$$

$$e^- + O_2 \rightarrow O_2^{-\bullet} \quad (6)$$

$$O_2^{-\bullet} + H_2O \rightarrow OH^- + HOO^\bullet \quad (7)$$

$$HOO^\bullet + H^+ \rightarrow OH^\bullet + OH^- \quad (8)$$

$$h^+ OH^- \rightarrow OH^\bullet \quad (9)$$

The major drawback for the AOPs is high energy consumption, especially when using UV lamps. The combination of solar AOP seems to be a cost-effective option to address this problem.

Large-scale solar collection is facilitated by the compound parabolic concentrator (CPC), which has been widely recognized as a practical choice for solar photochemical applications [19].

CPCs are fixed collectors with a reflective surface designed in the shape of an involute surrounding a cylindrical reactor tube. These designs have proven to offer optimal optics for low-concentration systems. Nearly all the direct and diffused UV radiation reaching the CPC can be captured and utilized within the reactor [20–22].

An artificial neural network (ANN) is a technique that simulates the biological neural network of the human brain to solve problems. ANNs can handle nonlinear problems and typically require less processing time than conventional mathematical methods.

A neural network comprises elements known as neurons, interconnected by a set of weights. Each neuron acts as a processing unit that receives multiple inputs, assigns weights to them, sums the weighted inputs, adds a bias, and then applies a transfer function to generate the neuron's output [23, 24]. A neural network is a parallel, interconnected structure that includes (a) an input layer, (b) hidden layers, and (c) an output layer. The input and output neurons correspond to the variables involved in prediction and those being predicted, respectively. Hidden layers serve as feature detectors, and theoretically, multiple hidden layers can exist. Their role is to transform inputs into a format that the output layer can utilize. The main steps in the artificial neural network process are learning, training, validation, and testing. The training phase involves presenting a series of input and output patterns to the neural network. During this phase, the weights of the connections between neurons are adjusted until the desired output is achieved for the given inputs. Through this process, the ANN learns the appropriate input and output responses. The ANN is then validated with input patterns that were not seen during training, enabling adjustments that improve the system's reliability and robustness. Validation also helps determine when to stop training to prevent overfitting. After training, the ANN is used to generate outputs based on a test data set. When the ANN produces output values within an acceptable range, it indicates successful training, and the ANN can be used as a predictive tool [25]. Neural Network Toolbox that came with MATLAB version 2021 was used in this work for ANN modeling.

The objective of this work is to study the effectiveness of solar AOPs in treating ATZ, ALC, and DIZ in solar homogeneous and heterogeneous photocatalytic systems, using a pilot-scale plant made up of CPC. Different dosages of H_2O_2, Fe^{+2}, and TiO_2 were tested to achieve the experimental objectives. An ANN model was used to predict the experimental results.

MATERIALS AND METHODS

Chemicals

In this research, three types of pesticides were used: ATZ, DIZ, and ALC. All pesticides were obtained in their commercial forms from Hebei Chinally International Trade Co., LTD. The purities of ATZ, DIZ, and ALC were 99%, 90%, and 94%, respectively. H_2O_2 with a purity of 35% was sourced from Hopkin and Williams. $FeSO_4 \cdot 7H_2O$ with a purity of 99.9% was purchased from Panreac. The pH of the solution was adjusted using H_2SO_4 and NaOH solutions. Sulfuric acid, with a purity of 97%, was obtained from Riedel-deHaën, while sodium hydroxide with a purity of 99% was sourced from BDH. Titanium dioxide P25, with a purity of 99%, was supplied by Himedia. All samples were prepared by dissolving the necessary quantities in distilled water.

Pilot plant and radiometer

The pilot plant used in this study was installed in the backyard of the Department of Environmental Engineering at Baghdad University, as shown in

Figure 1. It comprises a tank, a centrifugal pump, valves, piping, a flow meter, and solar collectors.

The tank has a capacity of 16 liters. The photoreactor comprises two borosilicate glass tubes with inner and outer diameters of 46.4 mm and 50.0 mm, respectively, and a length of 1.32 meters. Connection tubes made of PVC with a diameter of 62.5 mm facilitate flow. The irradiated volume inside the photoreactor is 5 liters. The collector features two compound parabolic collectors arranged in series on fixed supports inclined at 33°, aligned with Baghdad's latitude and facing south for optimal efficiency. These collectors are constructed from stainless steel plates coated with aluminum foil. A centrifugal pump of Reshani Pumps, circulates the solution at a flow rate of 1.4 m^3/h to maintain turbulent flow, monitored by a flow meter LZS Model. The solution's pH is adjusted using a German pH meter, WTW INOLAB 72. Global UV radiation powering the experiments is measured with a Sper Scientific Electronics Co. LTD ultraviolet radiometer, positioned at a 33° inclination facing south.

Experimental procedure

The experiments' durations were 90 minutes for homogeneous and 180 minutes for heterogeneous

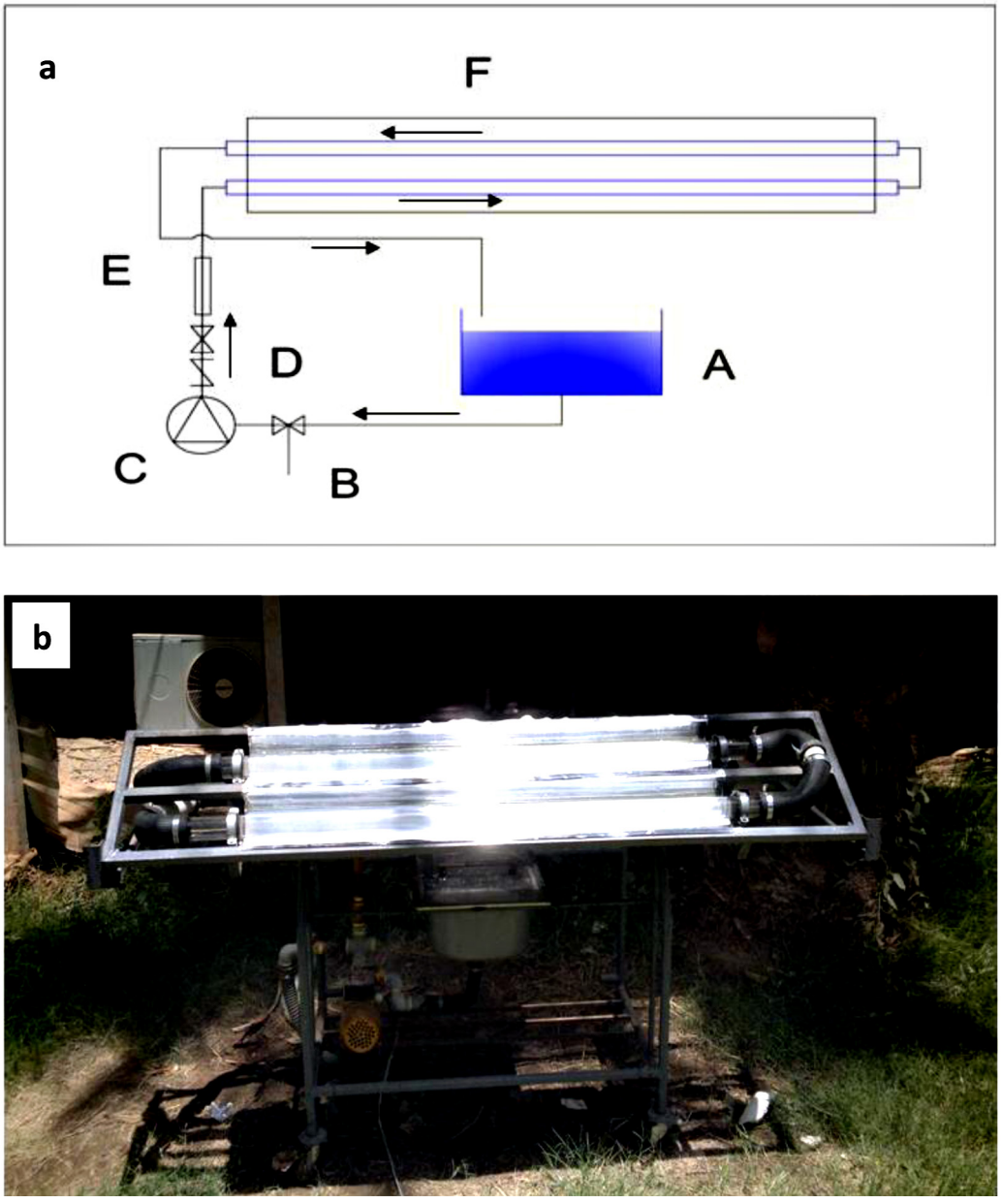

Figure 1. (a) Schematic representation of the pilot plant (A) tank, (B) drain valve, (C) pump, (D) Valve, (E) flow meter, (F) solar collectors (b) Pilot plant at the backyard of the Environmental Engineering Department

processes. Initially, the solar reactor was cleaned after filling with distilled water. To study the dark Fenton process, the solar collector was covered at the start of each experiment to prevent photochemical reactions. The required pesticide concentration was prepared beforehand and introduced into the pilot plant's tank, where it was recirculated for 15 to 30 minutes to ensure complete dissolution. The pH was adjusted to the desired level before adding Ferrous sulfate. After mixing for 15 minutes, hydrogen peroxide was added at specified concentrations to initiate the oxidation process. In the heterogeneous experiments, TiO_2 was added, and mixing continued for 45 minutes to allow pesticides to adsorb onto TiO_2 surfaces. Subsequently, hydrogen peroxide was introduced, and circulation was maintained for 15 minutes before removing the covers from the collectors, marking the start of the photo-Fenton degradation. Samples were collected at 15 and 30 minutes into the homogeneous and heterogeneous experiments, respectively. UV radiation levels were measured with a UV radiometer each time a sample was taken.

HPLC and COD analysis

The concentration of pesticides and intermediate products resulting from the oxidation reaction was measured using High Performance Liquid Chromatography (HPLC) of PerkinElmer series 200. The flow rate of the mobile phase was maintained at 1 mL/min. The stationary phase consisted of a C18 column (25 cm × 4.6 mm, 5 µm particle size) from Supelco, Discovery. A 0.2 µm syringe filter was used to filter the samples before analysis. The chemical oxygen demand (COD) of the samples was measured using a COD photometer system, which determined the total organic content in the solution during treatment. A sample volume of 2 mL was mixed with a digestion solution (MR-Rang: 0–1500 mg/L) containing mercuric sulfate, potassium dichromate, and sulfuric acid. A COD reactor model RD-125, Lovibond, was used to carry out the reaction at 150 °C for 120 minutes. The COD concentration was measured spectrophotometrically at 605 nm using a spectrophotometer of MD-100, Lovibond.

Standardized treatment time

The UV solar radiation intensity varies with the season, geographic location, and atmospheric conditions. Therefore, the duration of the photocatalytic treatment was standardized using 30 W/m², which represents the average intensity on a clear, sunny day [13]. The time t_{30W} was calculated as follows:

$$t_{30w,i} = t_{30w,i-1} + \Delta t_n \frac{UV\ V_R}{30V_T} \quad (10)$$

$$\Delta t_n = t_i - t_{i-1} \quad (11)$$

where: Δt_n represents the time between sample collections, UV refers to the average solar intensity (W/m²) over the sampling period, V_R and V_T denote the reactor volume and total liquid volume, respectively. This method ensures that the solar UV intensity remains unaffected by the time of year or geographic location during the experiments [26].

RESULTS AND DISCUSSION

Homogeneous solar photo-Fenton system

In the photo-Fenton system, Fe^{+2} and H_2O_2 were changed until the desired degradation efficiency was obtained. The experiments were maintained at pH = 2.9 to prevent iron precipitation [27, 28].

The initial stage in (Figure 2a) represents the dark Fenton reaction for ATZ. The mineralization was increased from 7% at $t_{30}w$ = 3.7 to 27% at $t_{30}w$ = 4.3 min when H_2O_2 concentration increased from 200 to 1200 mg/L. Stable iron complexes were formed in the dark Fenton reaction, which inhibits reaction with H_2O_2 these intermediate complexes dissociated with illumination [29]. For ATZ (20 mg/L) the H_2O_2 concentration was increased from 200 to 1600 mg/L reaching a maximum COD removal efficiency of 46% at 1600 mg/L after illumination time $t_{30}w$ = 19.75 min which is almost similar to the result obtained for 1200 mg/L with removal efficiency equal to 45% after t_{30w} = 20.5 min (Figure 2a). The initial concentration of 1200 mg/L was selected to be the best initial concentration of H_2O_2.

The improvement in removal efficiency can be attributed to the presence of Fe^{2+}, where the reactions between Fe^{2+} and H_2O_2, driven by solar irradiation, generate a greater number of $OH^{\bullet}$ radicals. These radicals are more effective in breaking down the pollutant's structure, leading to increased degradation. Further addition of H_2O_2 will decrease the overall reaction rate. At higher

H_2O_2 concentrations, the excess H_2O_2 molecules scavenge the valuable $OH^{\bullet}$ radicals generated by the direct photolysis of H_2O_2, leading to the formation of the much weaker oxidant $HO_2^{\bullet}$. Additionally, increased H_2O_2 concentrations may absorb and attenuate incident UV light, reducing its availability for the photocatalytic process [30–32]. The study examined how different initial Fe^{2+} concentrations (5, 10, 20, and 30 mg/L) influence the photo-Fenton process, using a fixed H_2O_2 concentration of 1200 mg/L. Figure 2b shows how COD removal efficiency varies with normalized illumination time (t_{30w}) for each Fe^{2+} level.

The mineralization efficiency increases to 45% with an iron concentration of 20 mg/L and reaches 46% at 30 mg/L. However, adding more iron reduces the degradation rate. Excessive iron levels cause turbidity and create dark areas within the photoreactor, decreasing its efficiency. This happens because some of the incoming light is scattered and cannot penetrate the photoreactor, leading to light loss [31, 32]. A comparison of the removal efficiency of ATZ and the mineralization of the pesticide under the best conditions of the photo-Fenton system is shown in (Figure 3a). By the end of the experiment, ATZ almost completely disappeared, reaching a removal efficiency of 95.7%, but there was no significant COD mineralization. The COD mineralization was only 45%.

The ATZ was identified after a retention time of 6.3 minutes in HPLC analysis (Figure 4a). Other peaks besides ATZ at t = 0 min appeared,

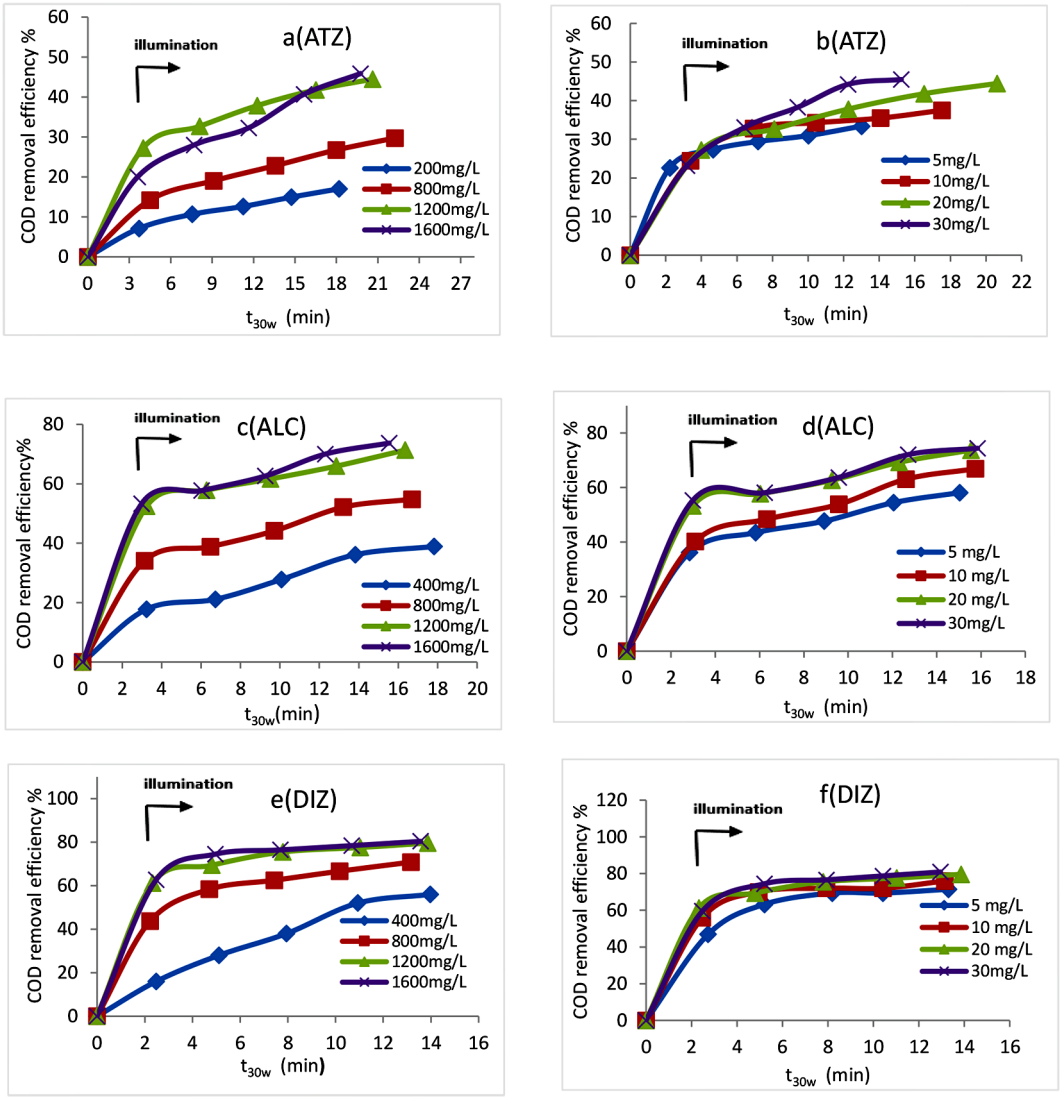

Figure 2. COD mineralization using homogeneous solar photo-Fenton system at pH=2.9, (a) the effect of initial H_2O_2 for ATZ at Fe^{+2}=20mg/L (b) the effect of initial Fe^{+2} for ATZ at H_2O_2=1200mg/L (c) the effect of initial H_2O_2 for ALC at Fe^{+2} =20 mg/L (d) the effect of initial Fe^{+2} for ALC at H_2O_2=1600 mg/L (e) the effect of initial H_2O_2 for DIZ at Fe^{+2}=20mg/L(f) the effect of initial Fe^{+2} for DIZ at H_2O_2=1200mg/L

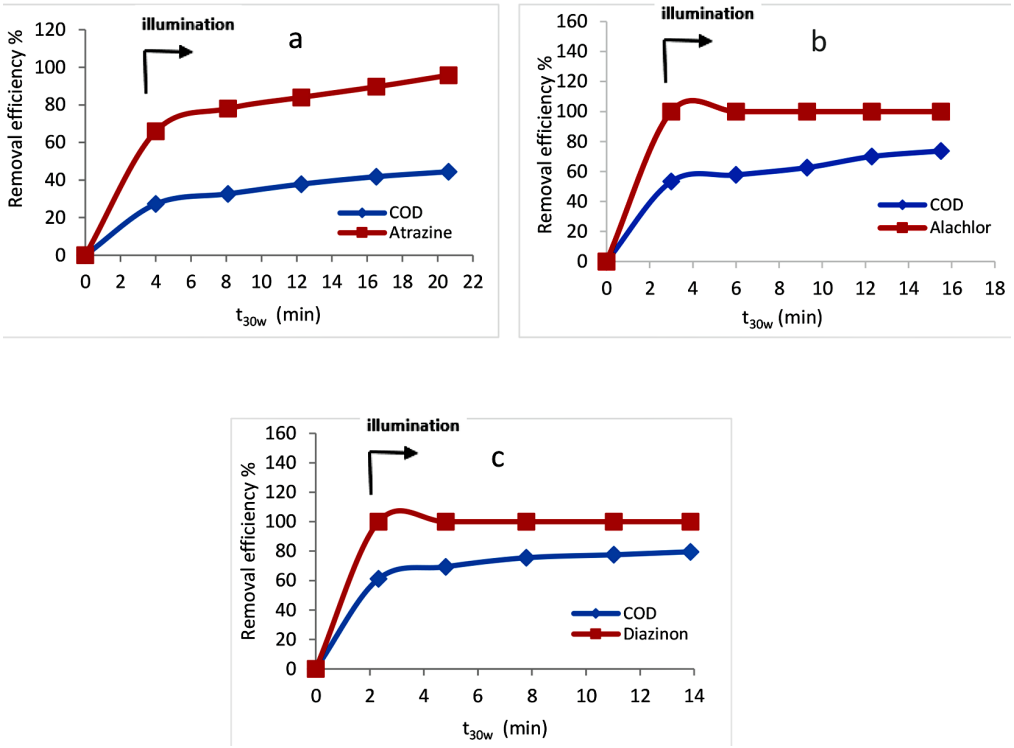

Figure 3. Comparison between the pesticides and COD removal efficiency using homogeneous solar photo-Fenton system at pH= 2.9 (a) ATZ at H_2O_2=1200 mg/L, Fe^{+2}=20 mg/L (b) ALC at H_2O_2=1600 mg/L, Fe^{+2}=20 mg/L, (c) DIZ at H_2O_2=1200 mg/L, Fe^{+2}=20 mg/L

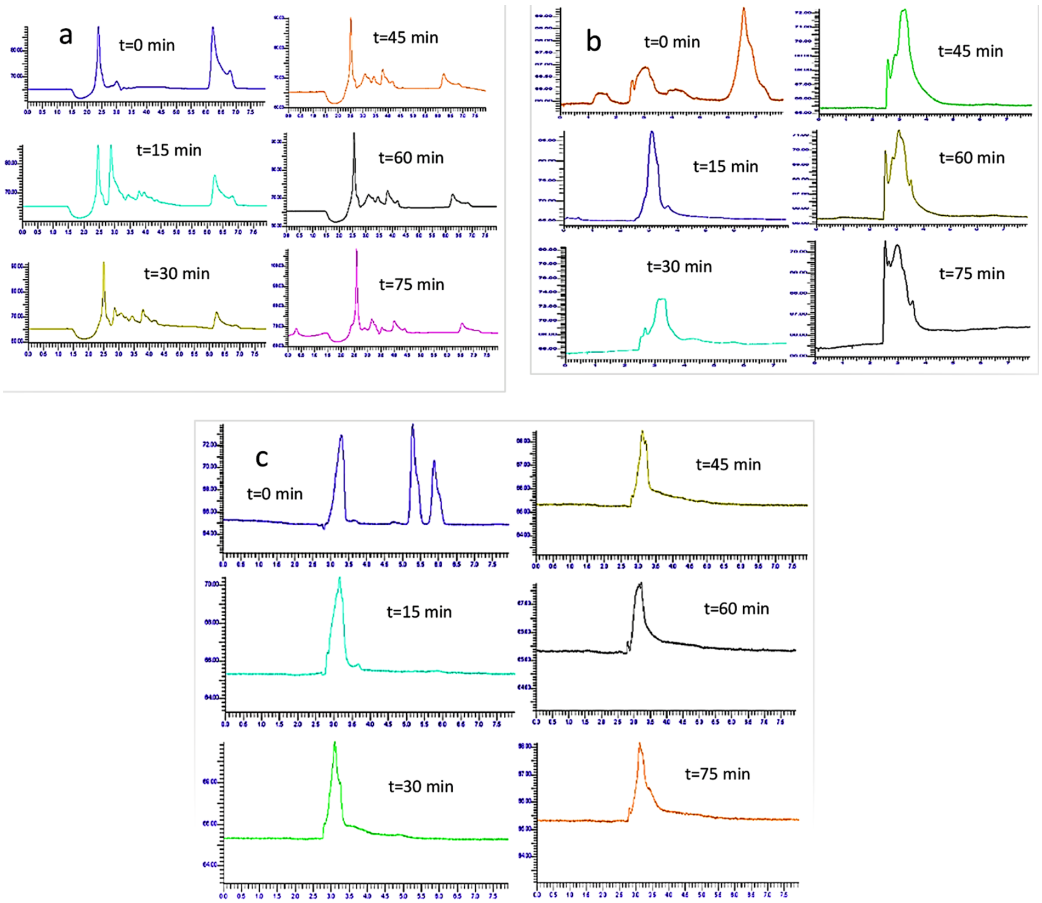

Figure 4. HPLC analysis for homogeneous photo-Fenton system at best conditions (a) ATZ (b) ALC (c) DIZ

which is due to the use of a commercial type of ATZ. The formation of reaction intermediates can be observed after 15 minutes of irradiation and continues until the end of the experiment.

The degradation pathway of atrazine (ATZ) leads to the formation of a final stable compound, cyanuric acid (2,4,6-Trihydroxy-s-triazine) [33]. Even though cyanuric acid is not entirely non-toxic, the World Health Organization's permitted limit in drinking water is 40 mg/L [10]. Cyanuric acid is biodegradable with negligible ecotoxicity, making the complete transformation of atrazine into cyanuric acid the most desirable treatment outcome [34].

The best mineralization efficiency of ALC (45 mg/L) was achieved at an initial H_2O_2 concentration of 1600 mg/L and 20mg/L of Fe^{+2}, resulting 74% when changing the H_2O_2 initial concentration at 400, 800, 1200, and 1600 mg/L and Fe^{+2} for 5, 10, 20, and 30 mg/L (Figure 2c and 2d).

A comparison between the removal efficiency of ALC and the COD mineralization of the pesticide under the best conditions is presented in (Figure 3b). ALC disappeared completely at illumination time (t_{30w} = 3 min). However, COD mineralization reached only 74% at the end of the experiment. ALC was detected at a retention time of 6.8 min (Figure 4b). It was completely eliminated during the photo-Fenton treatment in just 15 minutes. As irradiation continues, the formation and transformation of intermediate products can be observed.

The optimal mineralization efficiency for DIZ (30 mg/L) was achieved at Fe^{+2} = 20 mg/L and H_2O_2 = 1200 mg/L, reaching 80%. This was determined by varying H_2O_2 concentrations at 400, 800, 1200, and 1600 mg/L, and Fe^{+2} concentrations at 5, 10, 20, and 30 mg/L, as shown in (Figure 2e and 2f). A comparison between the removal efficiency of DIZ and the COD mineralization of the pesticide under optimal conditions is presented in (Figure 3c). DIZ was completely consumed at t_{30w} = 2.3 minutes, while the COD mineralization only reached 80% by the end of the experiment. DIZ can be identified by HPLC after a retention time of 6 minutes, as shown in (Figure 4c). The disappearance of DIZ was observed after 15 minutes of the oxidation process, while intermediate compounds continued to appear until the experiment ended.

Heterogeneous solar photocatalysis system

The solar heterogeneous photocatalysis method was applied to evaluate the feasibility of using TiO_2 for pesticide degradation. The optimal conditions for atrazine (ATZ) were identified as 300 mg/L of TiO_2, 2000 mg/L of H_2O_2, and a pH of 4.5, resulting in a 43% degradation rate. These parameters were determined by testing variations in TiO_2 concentrations (100, 200, 300, 400, and 500 mg/L) and H_2O_2 levels (800, 1200, 1600, 2000, and 2400 mg/L), as shown in Figures 5a and 5b. Additionally, the optimal pH was confirmed to be 4.5 after testing pH values of 4.5, 7, and 9.5, as illustrated in Figure 6a.

A comparison between ATZ concentration and COD mineralization using a heterogeneous solar photocatalyst system is shown in (Figure 7a). By the end of the experiment, the ATZ was reduced to 92%, while COD mineralization of ATZ reached only 43%. The increase in removal efficiency when changing TiO_2 dosage from 100 to 300 mg/L was attributed to the greater availability of active sites for photocatalytic reactions. However, at higher dosages such as 300 and 400 mg/L, the UV light intensity was diminished due to reduced penetration and increased scattering of solar light. This attenuation decreased the benefits of higher TiO_2 doses, leading to a decline in overall treatment performance. Additionally, high concentrations of TiO_2 promote particle agglomeration, which diminishes the available surface area for light absorption and consequently lowers the photocatalytic degradation rate [35–37]. The improvement in removal efficiency with varying H_2O_2 concentrations can be attributed to the rise in trapped electrons in the electron-hole pairs, leading to the production of more $OH^{\bullet}$ radicals for oxidation. However, increasing the H_2O_2 concentration beyond a certain point slows the degradation rate, as H_2O_2 reacts with these radicals, thus acting as an inhibiting agent [36].

For ALC, optimal conditions were achieved with H_2O_2 at 2000 mg/L, TiO_2 at 200 mg/L, and a pH of 4.5, as shown in Figures 5c, 5d, and 6b. A comparison between ALC disappearance and COD mineralization is presented in Figure 7b. By the end of the experiment, 96% of DIZ had disappeared, while 73% of COD mineralization was achieved.

For DIZ, optimal conditions were achieved with H_2O_2 at 1200 mg/L, TiO_2 at 200 mg/L, and pH 4.5, as shown in Figures 5e, 5f, and 6c. A comparison between DIZ disappearance and COD mineralization is presented in Figure 7c. Complete DIZ disappearance was achieved, while 76% COD mineralization was attained by the end of the heterogeneous treatment.

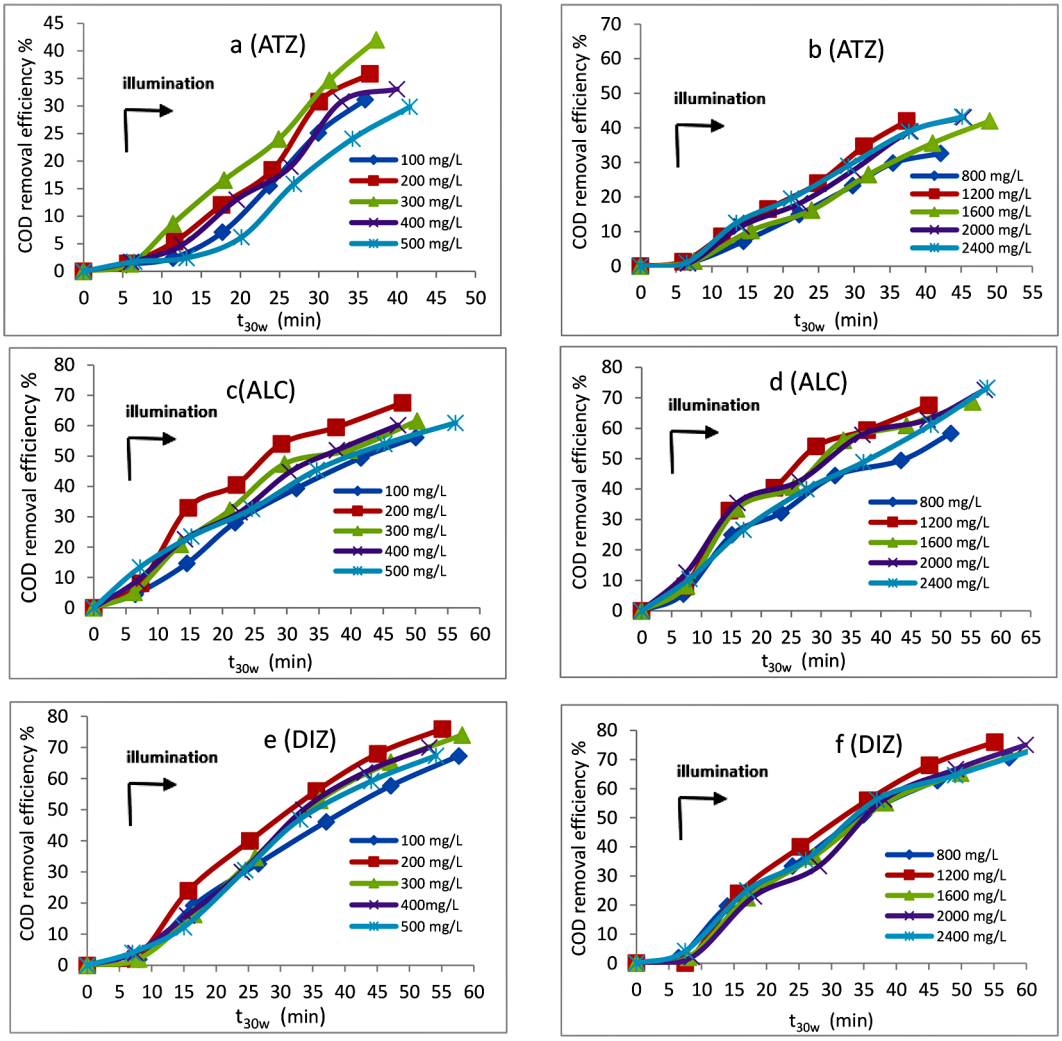

Figure 5. COD mineralization using heterogeneous solar photo-catalyst system at pH=4.5 (a) the effect of initial TiO_2 for ATZ at H_2O_2=1200 mg/L (b) the effect of initial H_2O_2 for ATZ at TiO_2=300 mg/L (c) effect of initial TiO_2 for ALC at H_2O_2= 1200 mg/L (d) the effect of initial H_2O_2 for ALC at TiO_2=200 mg/L (e)) the effect of initial TiO_2 for DIZ at H_2O_2=1200 mg/L (f) the effect of initial H_2O_2 for DIZ TiO_2=200 mg/L

A heterogeneous solar photocatalyst system appears to be less efficient than a homogeneous solar photocatalyst system. The results for both systems are summarized in Table 1. It can be observed that the mineralization efficiencies of 43%, 73%, and 76% were achieved with the heterogeneous system, compared to 45%, 75%, and 80% with the homogeneous system for ATZ, ALC, and DIZ, respectively. Additionally, an excess amount of the oxidant H_2O_2 and longer irradiation times were required. A heterogeneous solar photocatalyst system faces several challenges. These include the necessity to separate the TiO_2 suspension after treatment, incomplete degradation of substances adsorbed on the TiO_2 surface, which may require additional removal steps, longer degradation times compared to homogeneous systems, and increased costs due to the need for TiO_2.

Homogeneous solar photocatalyst treatment of mixtures of Atrazine, Alachlor, and Diazinon

Real wastewater usually contains a mixture of different pesticides. Consequently, after confirming the feasibility of treating each pesticide individually, mixtures of pesticides (ATZ, ALC, and DIZ) were treated in a homogeneous photocatalyst system. In the single-pesticide experiments, it was found that homogeneous solar photocatalyst treatment was the more efficient process. Therefore, all the current experiments were performed with initial Fe^{+2} = 20 mg/L, H_2O_2 = 1600 mg/L, initial concentration of pesticides (single or mixture) = 20 mg/L, and pH = 2.9.

The mineralization efficiency versus irradiation time for the single and mixed pesticides is

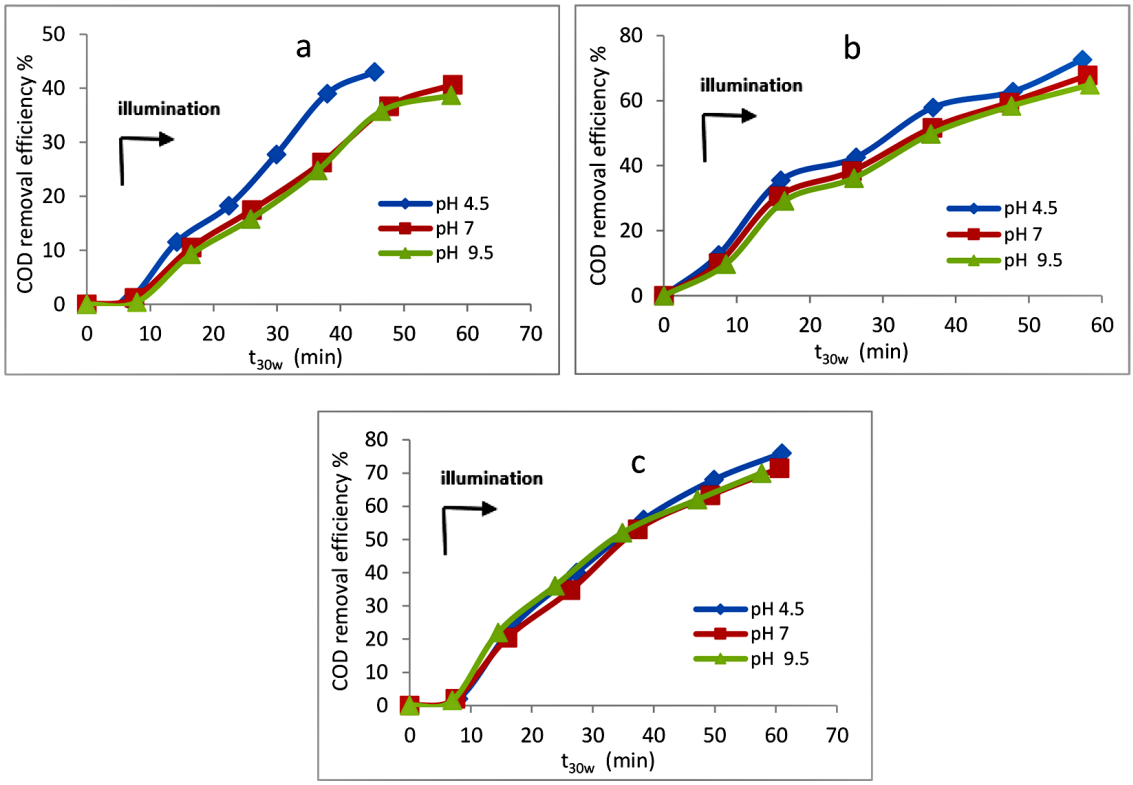

Figure 6. Effect of changing pH in heterogeneous solar photocatalyst system (a) ATZ at H_2O_2=2000 mg/L, TiO_2=300 mg/L (b) ALC at H_2O_2=2000 mg/L, TiO_2= 200 mg/L(c) DIZ at H_2O_2=1200 mg/L, TiO_2=200 mg/L

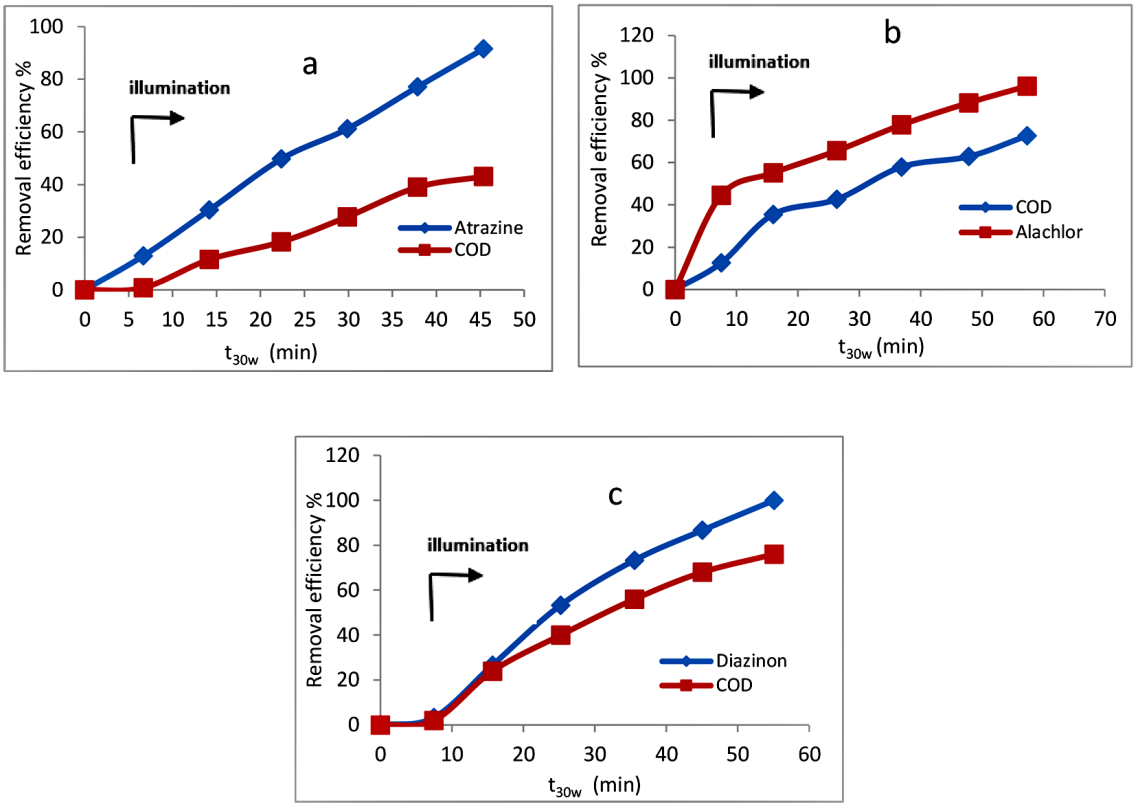

Figure 7. Comparison between the pesticides and COD removal efficiency using heterogeneous solar photocatalyst system at pH= 4.5 (a) ATZ at TiO_2=300 mg/L, H_2O_2=2000 mg/L (b) DIZ at TiO_2=200 mg/L, H_2O_2=1200 mg/L (c) ALC at TiO_2=200 mg/L, H_2O_2=2000 mg/L

Table 1. A comparison between homogeneous and heterogeneous solar photocatalyst systems for different pesticides

System	Details	Pesticides		
		ATZ	ALC	DIZ
Homogeneous	H_2O_2 (mg/L)	1200	1600	1200
	Fe^{+2} (mg/L)	20	20	20
	t_{30w} (min)	20.5	15.8	13.8
	Removal efficiency	45%	74	80%
Heterogeneous	TiO_2 (mg/L)	300	200	200
	H_2O_2 (mg/L)	2000	2000	1200
	t_{30w} (min)	45.3	57.3	55.1
	Removal efficiency	43%	73%	76%

shown in Figure 8. In the early stages of irradiation, a rapid increase in mineralization rate was observed, especially for ALC and DIZ. This is due to the nature of the pesticides and their intermediate products. After this period, the rate of mineralization slows down because of the persistence of recalcitrant products formed during oxidation, mainly carboxylic and aliphatic compounds, as well as the triazine ring derived from ATZ, which resist reaction with $OH^{\bullet}$ radicals. This leads to reduced degradation efficiency. Diazinon appears to be the most degraded pesticide, with COD mineralization efficiency reaching 80% at the end of the experiment.

The ATZ is the most resistant pesticide to reaction in this study. The COD mineralization efficiency was 45% by the end of the experiment. ATZ cannot be mineralized by AOP due to the stability of the triazine ring. ATZ reduces the oxidation in the mixture when combined with other pesticides. For a binary mixture (ALC and ATZ), the COD removal efficiency reaches 57% at the end of the experiment, compared to 74% for a solution of ALC alone at the same concentration (20 mg/L). Additionally, the presence of ATZ in a ternary mixture (ATZ, ALC, and DIZ) lowers the COD mineralization efficiency to 49% at the end of the experiment, compared with 74% and 80% for solutions of ALC and DIZ alone, respectively.

Artificial neural network for modelling solar AOPs

In the present study, an ANN structure of a three-layer artificial neural network was implemented as shown in (Figure 9), utilizing a tangent transfer sigmoid function (tan-sig) in the hidden layer and a linear transfer function (purelin) in the output layer, with the Levenberg-Marquardt backpropagation training algorithm. The input

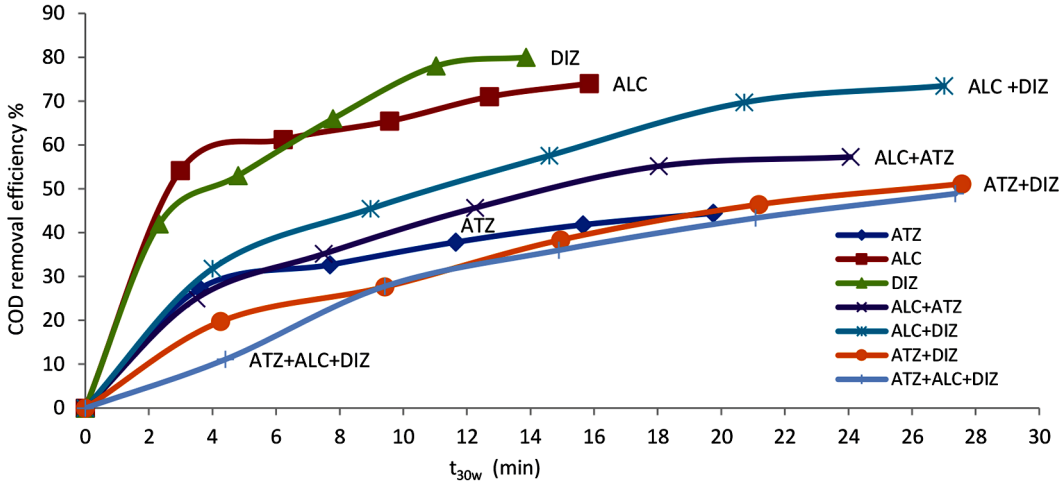

Figure 8. Homogeneous solar photocatalyst treatment of mixtures of ATZ, DIZ and ALC at Fe^{+2} =20 mg/L, H_2O_2=1600 mg/L and pH=2.9

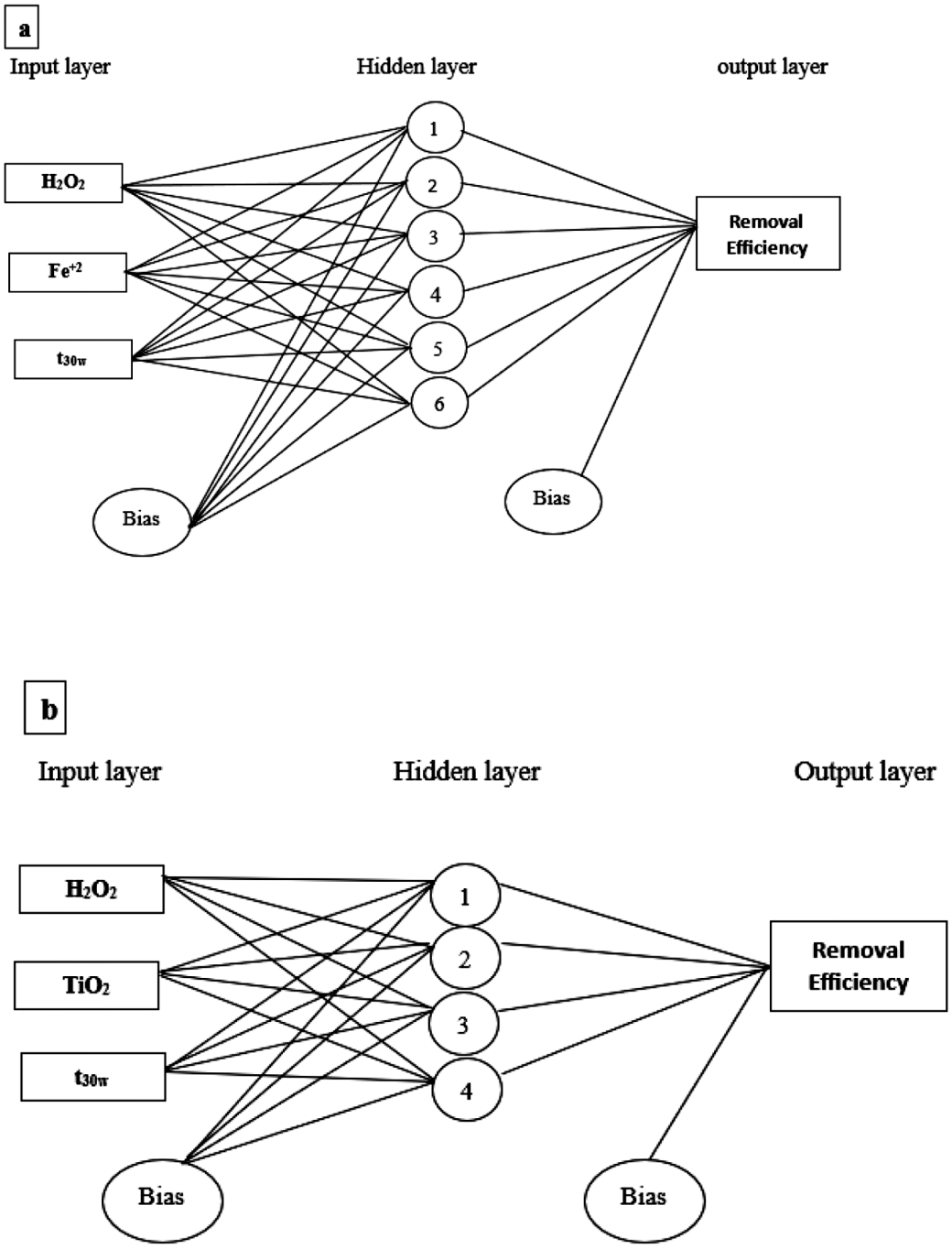

Figure 9. ANN structure (a) homogeneous solar photocatalyst system (b) for heterogeneous solar photocatalyst system

variables for the feed-forward neural network were H_2O_2, Fe^{2+}, and t_{30w} for the homogeneous system, and TiO_2, H_2O_2, and t_{30w} for the heterogeneous system. The output variable was the removal efficiency. The mean square error (MSE) was used to evaluate the network's performance, which was minimized with six neurons for homogeneous experiments and four neurons for heterogeneous experiments. Comparison between the calculated output values and the experimental results for the test sets showed a correlation coefficient above 0.981 under optimal conditions, indicating that the neural network model can effectively replicate the experimental data. The predicted results for the three pesticides are shown in Figures 10, 11, and 12, illustrating a strong agreement between the predicted and experimental data. Khataee and Kasiri [38], Elmolla and Malay [39], Roslan et al. [40], and Palma et al. [41] reviewed the applications of ANNs in modeling and simulating

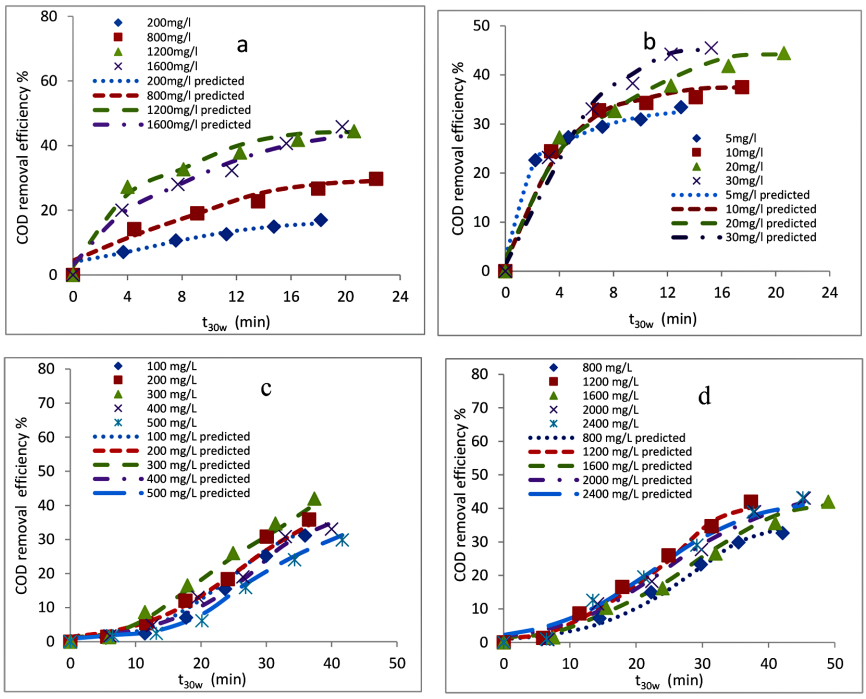

Figure 10. Artificial neural network model for predicting the experimental results for ATZ (a) solar photo-Fenton at different H_2O_2 (b) solar photo-Fenton at different Fe^{+2} (c) solar heterogeneous photo-catalysis at different TiO_2 (d) solar heterogeneous photo-catalysis at different H_2O_2

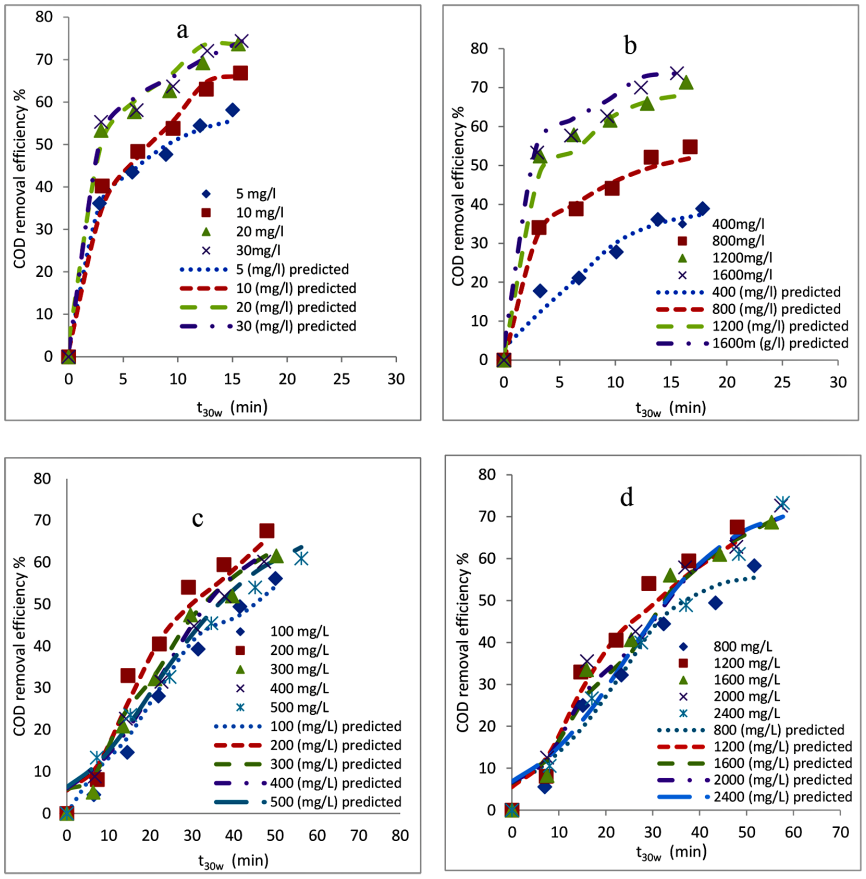

Figure 11. Artificial neural network model for predicting the experimental results for ALC (a) solar photo-Fenton at different Fe^{+2} (b) solar photo-Fenton at different H_2O_2 (c) solar heterogeneous photo-catalysis at different TiO_2 (d) solar heterogeneous photo-catalysis at different H_2O_2

photocatalytic processes in wastewater; their findings suggest that many researchers using the photo-Fenton treatment achieved a strong match between experimental and predicted output values, with a correlation coefficient exceeding 95%, as seen in this work.

CONCLUSIONS

In the present work, complete mineralization cannot be achieved due to the formation of intermediate products, which are the most difficult to degrade. In both systems – homogeneous and heterogeneous solar photocatalysis – ATZ is the slowest for mineralization, followed by ALC and DIZ. In a homogeneous solar photocatalyst system, the COD removal efficiency of ATZ under optimal conditions reaches 45% at t_{30w} = 20.5 min, compared to 74% at t_{30w} = 15.3 min and 80% at t_{30w} = 13.8 min for ALC and DIZ, respectively. This is due to the recalcitrant nature of the intermediate products formed from the parent pesticide. In a heterogeneous solar photocatalyst system, the best-case COD mineralization efficiencies are 43% at t_{30w} = 45.3 min for ATZ, 73% at t_{30w} = 57.3 min for ALC, and 76% at t_{30w} = 55.1 min for DIZ. The COD mineralization in the ternary mixture of ATZ, ALC, and DIZ was reduced to 49% at t_{30w} = 27.4 min. The results confirm that the ANN model can effectively predict the behavior of both systems.

Acknowledgements

The authors would like to thank Al-Bayan University for their support.

REFERENCES

1. Sharma A., Kumar V., Shahzad B., et al. Worldwide pesticide usage and its impacts on ecosystem. SN Applied Sciences. 2019; 1: 1446. https://doi.org/10.1007/s42452-019-1485-1
2. El-Nahhal I., El-Nahhal Y. Pesticide residues in drinking water, their potential risk to human health and removal options. Journal of Environmental Management. 2021; 299: 113611. https://doi.org/10.1016/j.jenvman.2021.113611
3. Mustafa Y. A., Mohammed S. J., Jabbar M. S. Adsorption of 2,4-Dichlorophenoxyacetic acid herbicide from aqueous solution by using cement kiln dust solid waste. Environmental Processes. 2024; 11: 34. https://doi.org/10.1007/s40710-024-00712-8
4. Wu X., Chen A., Yuan Z., et al. Atmospheric organochlorine pesticides (OCPs) and polychlorinated biphenyls (PCBs) in the Antarctic marginal seas: Distribution, sources and transportation. Chemosphere. 2020; 258: 127359. https://doi.org/10.1016/j.chemosphere.2020.127359
5. Garrido I., Fenoll J., Flores P., et al. Solar photocatalysis as a strategy for on-site reclamation of agro-wastewater polluted with pesticide residues on farms using a modular facility. Environmental Science and Pollution Research. 2021; 28(19): 23647–23656. https://doi.org/10.1007/s11356-020-10631-4
6. Natasha S. M., Khalid S., Murtaza B., et al. A critical analysis of wastewater use in agriculture and associated health risks in Pakistan. Environmental Geochemistry and Health. 2023; 45: 5599–5618. https://doi.org/10.1007/s10653-020-00702-3
7. Cleary J. A., Tillitt D. E., Vom Saal F. S., et al. Atrazine induced transgenerational reproductive effects in medaka (Oryzias latipes). Environmental Pollution. 2019; 251: 639–650. https://doi.org/10.1016/j.envpol.2019.05.013
8. Hu N., Xu Y., Sun C., et al. Removal of atrazine in catalytic degradation solutions by microalgae Chlorella sp. and evaluation of toxicity of degradation products via algal growth and photosynthetic activity. Ecotoxicology and Environmental Safety. 2021; 207: 111546. https://doi.org/10.1016/j.ecoenv.2020.111546
9. World Health Organization (WHO). Atrazine and its metabolites in drinking water: Background document for development of WHO guidelines for drinking-water quality (WHO/HSE/WSH/10.01/11/Rev/1). Geneva: Author. 2011.
10. World Health Organization (WHO). Guidelines for drinking-water quality (4th ed., incorporating the first and second addenda). Geneva: Author. 2022.
11. EPA. Drinking water standards and health advisories (EPA 822-R-06-013). Office of Water, U.S. Environmental Protection Agency. 2006.
12. Hubner U., Spahr S., Lutze H., et al. Advanced oxidation processes for water and wastewater treatment—Guidance for systematic future research. Heliyon. 2024; 10: e30402. https://doi.org/10.1016/j.heliyon.2024.e30402
13. Malato S., Blanco J., Cáceres J., et al. Photocatalytic treatment of water-soluble pesticides by photo-Fenton and TiO_2 using solar energy. Catalysis Today. 2002; 76: 209–220. https://doi.org/10.1016/S0920-5861(02)00220-1
14. Clarizia L., Russo D., Di Somma I., Marotta R., Andreozzi R. Homogeneous photo-Fenton processes at near neutral pH: A review. Applied Catalysis B: Environmental. 2017; 209: 358–371. https://doi.org/10.1016/j.apcatb.2017.03.011
15. Hong M., Wang Y., Lu G. UV-Fenton degradation of diclofenac, sulpiride, sulfamethoxazole

and sulfisomidine: Degradation mechanisms, transformation products, toxicity evolution and effect of real water matrix. Chemosphere. 2020; 258: 127351. https://doi.org/10.1016/j.chemosphere.2020.127351

16. Wang C., Zhang J., Du J., et al. Rapid degradation of norfloxacin by VUV/Fe^{2+}/H_2O_2 over a wide initial pH: Process parameters, synergistic mechanism, and influencing factors. Journal of Hazardous Materials. 2021; 416: 125893. https://doi.org/10.1016/j.jhazmat.2021.125893
17. Armaković S. J., Savanović M. M., Armaković S. Titanium dioxide as the most used photocatalyst for water purification: An overview. Catalysts. 2023; 13: 26. https://doi.org/10.3390/catal13010026
18. Gopalakrishnan G., Jeyakumar R. B., Somanathan A. Challenges and emerging trends in advanced oxidation technologies and integration of advanced oxidation processes with biological processes for wastewater treatment. Sustainability. 2023; 15: 4235. https://doi.org/10.3390/su15054235
19. Oller I., Malato S. Photo-Fenton applied to the removal of pharmaceutical and other pollutants of emerging concern. Green and Sustainable Chemistry. 2021; 29: 100458. https://doi.org/10.1016/j.cogsc.2021.100458
20. Rodrigues-Silva F., Starling M. C. V. M., Amorim C. C. Challenges on solar oxidation as post-treatment of municipal wastewater from UASB systems: Treatment efficiency, disinfection and toxicity. Science of the Total Environment. 2022; 850: 157940. https://doi.org/10.1016/j.scitotenv.2022.157940
21. Jiang C., Yu L., Yang S., et al. A review of the compound parabolic concentrator (CPC) with a tubular absorber. Energies. 2020; 13: 695. https://doi.org/10.3390/en13030695
22. Roccamante M., Salmerón I., Ruiz A., Oller I., Malato S. New approaches to solar advanced oxidation processes for elimination of priority substances based on electrooxidation and ozonation at pilot plant scale. Catalysis Today. 2020; 355: 844–850. https://doi.org/10.1016/j.cattod.2019.04.014
23. Kadioglu E. N., Ozturk H., Eroglu H., et al. Artificial neural network modeling of Fenton-based advanced oxidation processes for recycling of textile wastewater. Journal of Industrial and Engineering Chemistry. 2024; 136: 542–553. https://doi.org/10.1016/j.jiec.2024.02.045
24. Zhang C., Sun W., Wei W., et al. Application of artificial intelligence for predicting reaction results in advanced oxidation processes. Environmental Technology & Innovation. 2021; 23: 101550. https://doi.org/10.1016/j.eti.2021.101550
25. Elmolla E. S., Chaudhuri M., Eltoukhy M. M. The use of artificial neural network (ANN) for modeling of COD removal from antibiotic aqueous solution by the Fenton process. Journal of Hazardous Materials. 2010; 179(1–3): 127–134. https://doi.org/10.1016/j.jhazmat.2010.02.068
26. Jiménez M., Oller I., Maldonado M. I., et al. Solar photo-Fenton degradation of herbicides partially dissolved in water. Catalysis Today. 2011; 161: 214–220. https://doi.org/10.1016/j.cattod.2010.11.080
27. Pignatello J. J. Dark and photoassisted iron(3+)-catalyzed degradation of chlorophenoxy herbicides by hydrogen peroxide. Environmental Science & Technology. 1992; 26: 944–951. https://doi.org/10.1021/es00029a012
28. Mustafa Y. A., Shihab A. H. Removal of 4-chlorophenol from wastewater using a pilot-scale advanced oxidation process. Desalination and Water Treatment. 2013; 51(34–36): 6663–6675. https://doi.org/10.1080/19443994.2013.765362
29. Domingues E., Gomes J., Assunção N., et al. Iron-based catalysts under solar and visible radiation for contaminants of emerging concern removal. Energy Reports. 2020; 6: 711–716. https://doi.org/10.1016/j.egyr.2019.09.054
30. Chong M. N., Jin B., Chow C. W. K., et al. Recent developments in photocatalytic water treatment technology: A review. Water Research. 2010; 44: 2997–3027. https://doi.org/10.1016/j.watres.2010.02.039
31. Zhao T., Zheng M., Fu C., et al. Effect of low-level H_2O_2 and Fe(II) on the UV treatment of tetracycline antibiotics and the toxicity of reaction solutions to zebrafish embryos. Chemical Engineering Journal. 2020; 394: 125021. https://doi.org/10.1016/j.cej.2020.125021
32. Ali M. A., Maafa I. M., Qudsieh I. Y. Photodegradation of methylene blue using a UV/H_2O_2 irradiation system. Water. 2024; 16(3): 453. https://doi.org/10.3390/w16030453
33. Singh S., Kumar V. B., Chauhan A., et al. Toxicity, degradation and analysis of the herbicide atrazine. Environmental Chemistry Letters. 2018; 16: 211–237. https://doi.org/10.1007/s10311-017-0665-8
34. Rostami S., Jafari S., Moeini Z., et al. Current methods and technologies for degradation of atrazine in contaminated soil and water: A review. Environmental Technology. 2021; 24: 102019. https://doi.org/10.1016/j.eti.2021.102019
35. Ahmed S., Rasul M. G., Brown M. A., et al. Influence of parameters on the heterogeneous photocatalytic degradation of pesticides and phenolic contaminants in wastewater: A short review. Journal of Environmental Management. 2011; 92: 311–330. https://doi.org/10.1016/j.jenvman.2010.08.028
36. Fernandes A., Makoś P., Wang Z., et al. Synergistic effect of TiO_2 photocatalytic advanced oxidation processes in the treatment of refinery effluents. Chemical Engineering Journal. 2020; 391: 123488.

https://doi.org/10.1016/j.cej.2019.123488

37. Lama G., Meijide J., Sanromán A., Pazos M. Heterogeneous advanced oxidation processes: Current approaches for wastewater treatment. Catalysts. 2022; 12(3): 344. https://doi.org/10.3390/catal12030344
38. Khataee A. R., Kasiri M. B. Artificial neural networks modeling of contaminated water treatment processes by homogeneous and heterogeneous nanocatalysis. Journal of Molecular Catalysis A: Chemical. 2010; 331(1–2): 86–100. https://doi.org/10.1016/j.molcata.2010.07.016
39. Elmolla E. S., Malay C. The use of artificial neural network (ANN) for modelling, simulation and prediction of advanced oxidation process performance in recalcitrant wastewater treatment. 2011. https://doi.org/10.5772/14920
40. Roslan N. N., Lau H. L. H., Suhaimi N. A. A., Shahri N. N. M., Verinda S. B., Nur M., Lim J.-W., Usman A. Recent advances in advanced oxidation processes for degrading pharmaceuticals in wastewater—A review. Catalysts. 2024; 14(3): 189. https://doi.org/10.3390/catal14030189
41. Palma D., Antela K. U., Bianco Prevot A., Cervera M. L., Morales-Rubio A., Sáez-Hernández R. Artificial neural networks applied to photo-Fenton process: An innovative approach to wastewater treatment. Water Science and Engineering. 2025; 18(3): 324–334. https://doi.org/10.1016/j.wse.2025.04.005